ELSEVIER

Styles of volcano-induced deformation: numerical models of substratum flexure, spreading and extrusion

Benjamin van Wyk de Vries [*], Ray Matela

The Open University, Walton Hall, Milton Keynes MK7 6AA, UK

Abstract

The gravitational deformation of volcanoes is largely controlled by ductile layers of substrata. Using numerical finite-element modelling we investigate the role of ductile layer thickness and viscosity on such deformation. To characterise the deformation we introduce two dimensionless ratios; Π_a (volcano radius/ductile layer thickness) and Π_b (viscosity of ductile substratum/failure strength of volcano). We find that the volcanic edifice spreads laterally when underlain by thin ductile layers ($\Pi_a > 1$), while thicker ductile layers lead to inward flexure ($\Pi_a < 1$). The deformation style is related to the switch from predominantly horizontal to vertical flow in the ductile layer with increasing thickness (increasing Π_a). Structures produced by lateral spreading include concentric thrust belts around the volcano base and radial normal faulting in the cone itself. In contrast, flexure on thick ductile substrata leads to concentric normal faults around the base and compression in the cone. In addition, we show that lower viscosities in the ductile layer (low Π_b) lead to faster rates of movement, and also affect the deformation style. Considering a thin ductile layer, if viscosity is high compared to the failure strength of the volcano (high Π_b) then deformation is coupled and spreading is produced. However, if the viscosity is low (low Π_b) substratum is effectively decoupled from the volcano and extrudes from underneath it. In this latter case evidence is likely to be found for basement compression, but corresponding spreading features in the volcano will be absent, as the cone is subject to a compressive stress regime similar to that produced by flexure. At volcanoes where basement extrusion is operating, high volcano stresses and outward substratum movement may combine to produce catastrophic sector collapse. An analysis of deformation features at a volcano can provide information about the type of basement below it, a useful tool for remote sensing and planetary geology. Also, knowledge of substratum geology can be used to predict styles of deformation operating at volcanoes, where features have not yet become well developed, or are obscured. © 1998 Elsevier Science B.V.

Keywords: volcano; gravitational; deformation; substratum; flexure; spreading; extrusion

1. Introduction

Individual volcanoes and collective volcanic masses load the crust and the resulting stresses can cause significant deformation, including thrusts, rifts, (van Bemmelen, 1970; Borgia et al., 1990; van Wyk de Vries and Borgia, 1996) and sector collapse (van Wyk de Vries and Francis, 1997). The gravitational stresses can also combine with the regional stress field resulting in modified regional deformation patterns (Cyr and Melosh, 1993; van Wyk de Vries and

* Corresponding author. Tel.: +44-1908-652558; fax: +44-1908-655151; e-mail: b.van-wyk-de-vries@open.ac.uk

Merle, 1996a). The style of deformation caused by volcano loading is largely dependant on the type of substratum and especially the presence of ductile layers beneath a cone (Nakamura, 1980; Borgia, 1994; van Wyk de Vries and Borgia, 1996; Merle and Borgia, 1996).

In Fig. 1 we present natural examples of volcano-induced deformation that illustrate two contrasting types of behaviour: spreading and flexure. The first pair of examples are from areas of low tectonic stress, where volcano-induced deformation is dominant (Fig. 1a and b). At Concepción (Fig. 1a) spreading is characterised in the basement by concentric thrust faults and diapirs and in the cone by radial normal faults. In contrast, at Iwaki (Suzuki, 1968), flexure is characterised by a broad bulge around the base and by normal faults in the substratum orientated concentric to the cone. In contrast to Concepción no extensional faulting is found on the cone (Fig. 1b).

The second pair of examples are taken from extensional rifts (Fig. 1c and d). In this type of situation, the regional extensional stress is modified locally by the volcano load, and the orientation of the regional parallel normal faults is diverted. Fieale has faults which curve in toward the volcano (Fig. 1c), interpreted as a spreading response coupled with regional extension (van Wyk de Vries and Merle, 1996a). This has been called an 'hourglass', or 'bowtie' fault pattern (De Chabalier, 1993; De Chabalier and Avouac, 1994). In contrast, Fantale (Fig. 1d) has faults which curve around the volcano, in what we call a wristwatch style. This may be flexure operating in an extensional environment.

Similar features to Fantale have been described at Alba Patera, Mars (Turtle and Melosh, in press) and around Venusian coronae (Cyr and Melosh, 1993). Fault patterns similar to Fieale have also been described at Axial Seamount (van Wyk de Vries and Merle, 1996a), Hengil, Iceland (van Wyk de Vries and Merle, 1995), Iceland itself (van Wyk de Vries and Merle, 1996b), and at Venusian volcanoes, where they have been called 'arachnids'.
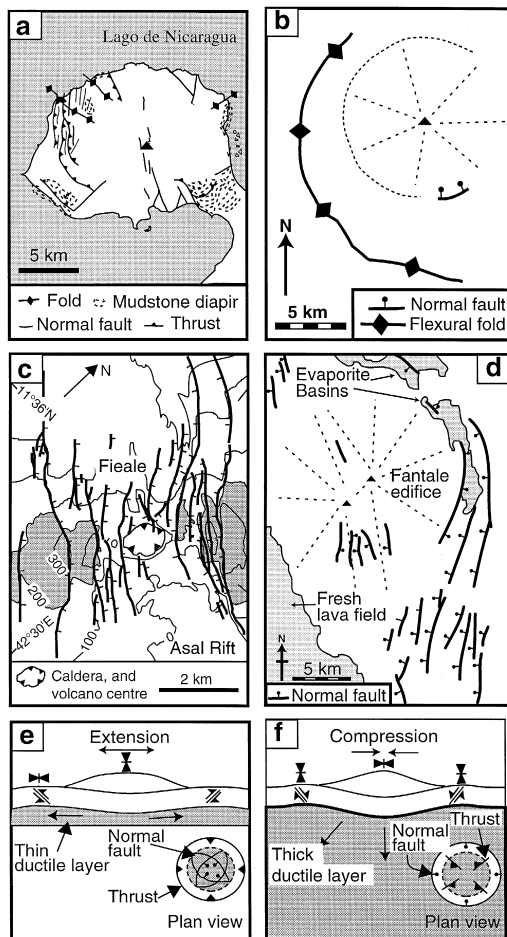
Fig. 1. Examples of volcanoes with contrasting fault patterns and two hypotheses explaining the patterns. The first two are volcanoes that are subjected to low tectonic stress, the second two are under regional extension in the active Ethiopian rift. (a) Concepción, Nicaragua after van Wyk de Vries and Borgia (1996): this volcano stands on thick lake sediments. Thrusting extends around the western base, while diapirs emerge around the eastern side. (b) Iwaki volcano, after Suzuki (1968): this cone is surrounded by a broad flexural fold, about 5 km from the edifice, and concentric normal faulting at the base of the cone. (c) Fieale volcano, Asal rift, after De Chabalier (1993). At Fieale the faults curve into the volcano: the opposite to Fantale. (d) Fantale, Afar rift, from Landsat TM Images. At this volcano normal faults bend around the eastern side deviating from the regional N–S trend. There is a small intra-volcano rift on the south flank. (e) Volcanic mass standing on brittle crust with a thin ductile layer (after Merle and Borgia, 1996). Here the mass induces radial spreading i.e. extension in the cone and compression in the surrounding area. Inset shows the expected fault pattern. (f) Volcano-induced flexure of an elastoplastic layer on top of an infinitely thick ductile layer causes compression in the structure and extension at the margins (after Cyr and Melosh, 1993).

In the case of Iwaki, Concepción and Fieale various authors have interpreted the deformation as a response of ductile substratum to the volcanic load (Suzuki, 1968; van Wyk de Vries and Borgia, 1996; and van Wyk de Vries and Merle, 1996a). We suggest that the two contrasting styles of flexure and spreading described above are dependant on different ductile substratum parameters, such as thickness and/or viscosity.

In this paper we investigate the role of rock viscosity and ductile layer thickness on the stress state and style of deformation at volcanoes by a simple analogue model and a finite-element approach. We use a fluid base and an elastoplastic upper plate and cone. We unify the models of spreading on a thin fluid layer as illustrated in Fig. 1e (Merle and Borgia, 1996) with that of flexure on a thick, unconstrained fluid base as shown in Fig. 1f (Cyr and Melosh, in press). The results are then used to explain the spreading, extruding and flexural deformation styles described above.

2. The analogue model

We constructed a simple analogue experiment to test the effect of changing the thickness of a ductile layer below a cone (Fig. 2). The layer was constructed out of golden syrup contained in a flat bottomed glass bowl, on top of which a cone of

sugar was emplaced. The model was not scaled, but served as a useful guide to the following numerical experiments. When a thin layer of golden syrup is used, the sugar cone spreads outwards, rapidly changing from a cone to a shield. With a thicker layer a slight amount of spreading is observed, but the cone retains a conical shape. With a very thick layer the cone does not noticeably change shape, although its base can be seen sagging into the underlying syrup. This model shows that a thin ductile layer results in spreading, whereas a thick layer results in sagging.

The ratio of volcano diameter: ductile layer thickness (L/T) is a dimensionless Π-number (Middleton and Wilcock, 1994), which we term Π_a. In our analogue experiment presented here, a high Πa is characteristic of spreading, while a low Π_a indicates that flexure will operate. The division between the two occurs at about $\Pi_a = 1$, i.e. where the ductile layer thickness is half the diameter of the cone.

3. The numerical model

Previous models investigating volcano induced stress have either been numerical (Cyr and Melosh, 1993; van Wyk de Vries and Borgia, 1996), or physical analogue (Merle and Borgia, 1996; van Wyk de Vries and Merle, 1996a). Here we use a numerical approach (finite element analysis) in which
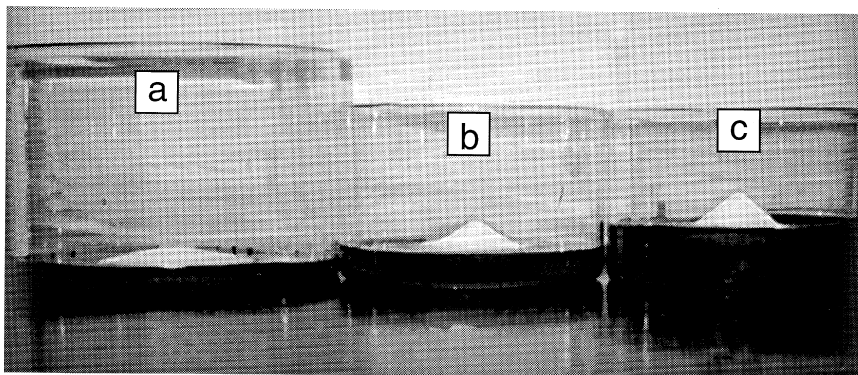
Fig. 2. Simple analogue experiment of a cone on a viscous layer. Viscous layer is golden syrup and the cone is granulated sugar. (a) Cone on thin layer, the cone spreads (Π_a about 12). (b) On thicker layer: the cone spreads a small amount and sinks into the fluid (Π_a about 1). (c) On very thick layer: the cone only sags into crust (Π_a about 0.5).

our models are influenced by our analogue model described above. Our approach is similar, in general, to many loading studies in civil engineering (e.g. De Borst, 1982; Zienkiewicz, 1977). This study differs from these in three main aspects: (1) The scale, which is at least ten times greater in length, 1000 × greater in the forces, and 1,000,000 × greater in the time scales involved. (2) The inclusion of a viscous layer, and consequent time-dependent deformation. (3) The fact that the edifice is deformable entity in the analysis, and not simply a rigid load.

Our numerical analysis is constructed with a geometry and rheology that differs to those used in the published analogue experiments, as we use an elastic-perfectly plastic solid, rather than a brittle material. In addition our models are scaled to natural dimensions. This work provides information about the stress and displacement states in both analogue and natural situations in so far as previous analogue models were well scaled to simulate nature. For a discussion of the analogue scaling see Merle and Borgia (1996).

3.1. Methodology

Numerical modelling using the finite-element method has three distinct steps: preprocessing, solution and post processing. Typically the preprocessing stage comprises some 70% of the time required for analysis. The main function of this preprocessor stage is the creation of a suitable finite-element model. According to Baguley and Hose (1994) this must include the following: (1) The definition of the fundamental geometry of the structure. (2) The breaking down of the structure into (finite) elements, usually defined geometrically by the coordinates of nodes on their boundaries. (3) The definition of the connectivity of the elements in the structure. (4) The definition of the material and geometric properties of the elements. (5) The definition of the loading. (6) The definition of the supports.

3.2. Geometry

The geometrical model is an abstraction of the physical reality, but must approximate as closely as possible the geometry of the physical problem. Our

geometry was influenced by the analogue experiments which have successfully approximated the volcano-substratum system (Fig. 3). The final geometrical models presented here are the outcome of many iterations during which our main problem was the modelling of the cone and the cone-substrate interface. Initial models of the cone were truncated triangles as illustrated in Fig. 3b, and were similar to those used by van Wyk de Vries and Borgia (1996). Although these accurately modelled the cone compo-
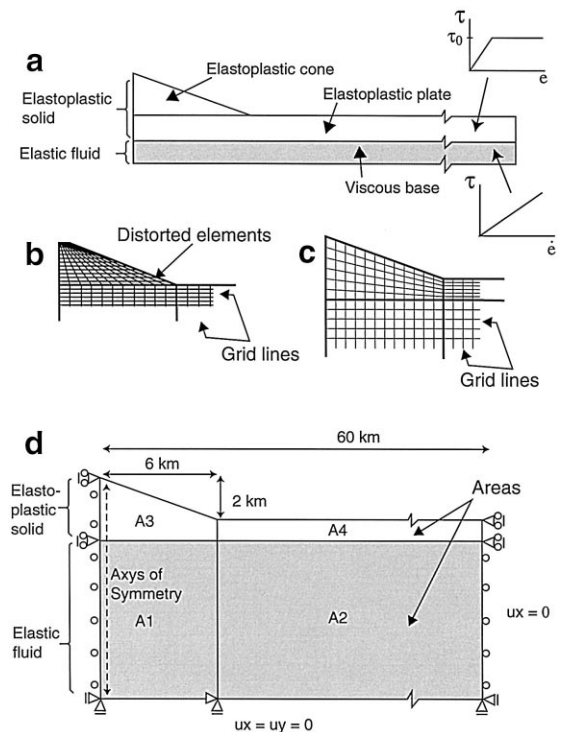
Fig. 3. Model geometry and properties. (a) Generalised diagram of model strategy, showing main components and physical parameters. (b) Example of previous models mesh used by van Wyk de Vries and Borgia (1996) for comparison with our better shaped elements in (c). (c) Inset showing mesh elements in cone and elastoplastic upper plate component (areas 3 and 4). The Cone (area 3) contained 100 elements, with a mesh of 10 vertical nodes and 10 horizontal nodes. Area 4, the elastoplastic plate, contained 1080 nodes: 10 along the vertical edge and 108 on the horizontal. The number of vertical mesh lines in the viscous layer was the same as in the upper layer, and the horizontal lines were 200 m for a 1-km layer and or 500 m for thicker layers. (d) Finite-element model construction: the geometry of the model adopted for this study, showing dimensions, boundary conditions and model areas (A1–A4).

nent, they caused problems when applying a quadrilateral mesh. This is because the quadrilateral elements had to be highly distorted in order to fit within a nearly triangular geometry. We overcame this problem by constructing a new geometrical model. It is assembled from four areas in which the cone and part of the upper plate form one single area (Fig. 3c). The four areas, one quadrilateral and three rectangular, are much more suited to meshing with pure quadrilateral elements. The first two areas, i.e. A1 and A2, define the contained fluid base, and the other two, A3 and A4, define the elastoplastic volcano and upper plate component (Fig. 3d). This geometry is close to that used in the analogue experiments of Merle and Borgia (1996), where the cone and upper plate are constructed of the same material.

The cone is 2000 m high and 6000 m wide giving an initial slope angle of 18°, a reasonable average for most volcanoes. The elastoplastic layer thickness was taken to be 1000 m deep in the first set of experiments, and then was changed to 2000 m depth. The fluid layer depth was varied from 1000 to 20,000 m. The far field edge of the model was set at 60,000 m with the cone side as the axisymmetric axis of rotation. In other words we looked at a planar axisymmetric slice through the volcano.

3.3. Material properties

The cone and upper plate areas are modelled with a nonlinear Drucker–Prager elastic-perfectly plastic material. This combines the von Mises yield criterion with the Mohr–Coulomb failure criterion to give an elastic-perfectly plastic material, with dependence on hydrostatic stress. The Drucker–Prager material is therefore well suited to studies of geological situations and it provides the closest approximation to the real geological properties of the cone and top layer that we have available at this time. While we cannot produce discrete faults in finite element analysis, the inclusion of plasticity allows us to model a yield strength, and thereby approximate fault induced deformation in the continuum. Rate-independent plasticity is characterised by the irreversible straining that occurs in the material once a certain level of stress is reached. The plastic strains are assumed to develop instantaneously, i.e. independent of time.

The fluid base areas are modelled with a viscous material. This material includes the isotropic material properties: fluid elastic Modulus (bulk Modulus of the fluid), viscosity and density. The fluid material model can both closely simulate the behaviour of silicone in analogue experiments and support viscosities encompassing those of real rocks (10^{17}–10^{22} Pa · s.). As with real rocks, the model fluid also has elastic properties, but since the program regards it as a fluid, no stresses can be determined. As we are primarily concerned with displacement in the viscous layer, and stresses within the volcano and plate, stress retrieval in the 'fluid' layer was not a concern.

Physical parameters used in the modelling are given in Table 1. The cone and upper plate density was taken to be that of porous volcanic products (lava flows and tephra) and of coarse sediments. The

Table 1
Model parameters, units and values used in the experiments

Element	Parameter	Model 1	Model 2	Model 3
Solid	density (kg m^{-3})	2200	2200	2200
	Poisson's ratio (-)	0.20	0.20	0.20
	Young's modulus (Pa)	2×10^{10}	2×10^{10}	2×10^{10}
	shear modulus (Pa)	8.0×10^{9}	8.0×10^{9}	8.0×10^{9}
Plane 42	bulk modulus (Pa)	1.33×10^{10}	1.33×10^{10}	1.33×10^{10}
	angle of friction (°)	30°	30°	30°
	coherence (Pa)	9.0×10^{6}	9.0×10^{6}	9.0×10^{6}
	dilatency (°)	20	20	20
Fluid	density (kg m s^{-1})	2700	2700	2700
	Poisson's ratio (-)	0.20	0.20	0.20
Fluid 79	bulk modulus (Pa)	1.33×10^{10}	1.33×10^{10}	1.33×10^{10}
	viscosity (Pa · s)	$5 \times 10^{18-22}$	5×10^{20}	5×10^{20}
Geometry	plate (km)	1	1	2
	base (km)	1	1,2,5,10,20	1,2,5,10,20

lower layer was given a higher density to simulate more compact nonporous rock. Elastic moduli are similar to those used in other numerical studies (i.e. Borgia et al., 1994; van Wyk de Vries and Borgia, 1996). The angle of friction was taken to be 30°, an average value for rocks, and that used in analogue experiments. The cohesion was taken to be 9×10^6 Pa. This value is probably at the high end for volcanic strata, representing lavas, or consolidated lava/tephra sequences, but is within the range of other crustal rocks. This high value was necessitated by the appearance of numerical instabilities in the program at lower values. The fluid was given similar elastic moduli to the upper plate solid, and the viscosity was varied from 10^{17} to 10^{22} Pa·s, encompassing the range found in diverse rocks from claystones, massive lavas and intrusives, to aesthenospheric and lithospheric mantle.

3.4. Elements

Using the program ANSYS©5.3, we meshed the volcano cone and upper plate areas with a PLANE42 element and the contained fluid base areas with a FLUID79 element (ANSYS, 1996). Both of these axisymmetric quadrilateral elements are defined by four nodes having two degrees of freedom per node, i.e. translations in the nodal x and y directions. The PLANE42 element also supports plasticity, creep, large deflection, and large strain. The FLUID79 element on the other hand, is a modification of the PLANE42 element used primarily to model fluids contained within vessels having no net flow rate. It does not support large deflections. This caused some initial problems around the interface between the relatively stiff cone upper-plate component and the fluid substrate. We overcame these problems by mesh refinement and load/time step manipulation (Table 2). While a quadratic element for the cone would have produced a more accurate solution, the linear element used provided a reasonable solution at a much lower cost. This was important as the larger models took several days of computation. Ideally, for a more detailed analysis of individual volcanoes, rather than the general ones used here, we need to use a quadratic isoparametric element capable of supporting viscoelasticity and stress stiffening. Unfortunately, while this element is available to us in

Table 2
Mesh properties for models of various ductile base thicknesses and an elastoplastic plate of 1000 m

	Thickness of T			
	1000	5000	10,000	20,000
Mesh property				
Nodes	1089	2057	3267	5587
Elements	960	1920	3120	5520
Degrees of freedom	1920	3840	6240	11,040

ANSYS, the required geological material data is not available for the geological phenomena being modelled.

3.5. Mesh

As stated above, we constructed the model mesh from the four areas (Fig. 3d), this particular geometry minimised the associated aspect ratio problems caused by the use of pure quadrilateral elements in a triangular cone shape. For the purposes of this analysis the solid upper plate and cone were considered as one component as they shared the same material.

The number of elements and nodes, and thus the total degrees of freedom, varied between models, depending upon the depth of the fluid layer and the thickness of the upper plate (Table 2). For the 1000 m plate model there were approximately 2178 degrees of freedom while in the 20,000 m model there were approximately 11374 degrees of freedom. We were concerned about the mesh density in the area of the cone and its substrate. To test the accuracy of our mesh, we created another model that quadrupled the mesh density in this area, and doubled it in the rest of the model. For the unaveraged stress and for maximum displacement values the difference was less than 1%. Tables 1 and 2 give details of the various models and their mesh properties.

3.6. Boundary conditions

The boundary conditions were consistent for all models and are illustrated on Fig. 3a. The far field side is restrained in *ux*, the base is fully restrained in *ux* and *uy*, while the left hand side is an axis of symmetry. The fully restrained fluid base represents a no-slip condition and as such simulates flow against

a wall, i.e. the velocity components at the wall are zero. The only load is that of acceleration due to gravity.

3.7. Analysis

The initial models were run as a nonlinear static analysis. Although this form of analysis is capable of supporting inertial loads (due solely to gravity), these loads cannot vary with time, i.e. static loading conditions. This caused some problems as the fluid elements were not capable of supporting large deflections and in some cases 'crumpled' under the load. To get over some of these problems and to simulate a more realistic loading scheme, we turned to nonlinear transient analysis. This mode of analysis gave us the tools to model the fluid response to time-varying inertial loads.

3.8. Runs

To simulate the emplacement of the volcano in our early models, the cone area was given an initial near zero density and the model was loaded with gravity. The simulation proceeded for a small period of time, in the region of 1 yr. This allowed pure elastic effects to take place. The cone density was then raised in 500 kg m^{-3} steps over 500 yr time steps, thus growing the volcano in 2000 yr. Once loaded the model was left to run for up to 2 million years in time steps determined by the various input parameters and solution options chosen.

In our most recent models the gravity load was applied to the whole model at the start, as we found that this did not significantly affect the final solution. The loading sequence was as follows: 1 yr, 1000 yr, 10,000 yr and finally 10,000 yr increments to a total of 2 million years. This gave us the transient solutions at these various time steps. We were then able to analyse the viscous response by subtracting out the first, i.e. 1 yr solution, which contained the elastic loading effects, from the remaining time steps. The loads themselves were applied as stepped loads in that the full value was applied at the first substep and held constant for the rest of the load step.

In all these cases automatic time (load) stepping was employed. That is to say, both time step predic-

tion and time step bisection were used (ANSYS, 1996). Both Newton–Raphson and preconditioned conjugate gradient solvers were used to solve the nonlinear equations associated with the transient analysis.

3.9. Problems

Most of the problems we encountered arose because of the difference in stiffness between the cone-plate component and the fluid base. This was a continuous source of numerical instability. In most cases we were able to overcome this by decreasing the time (load) step. The system also proved to be sensitive to cohesion, restricting us to the higher end of natural and analogue cohesion values.
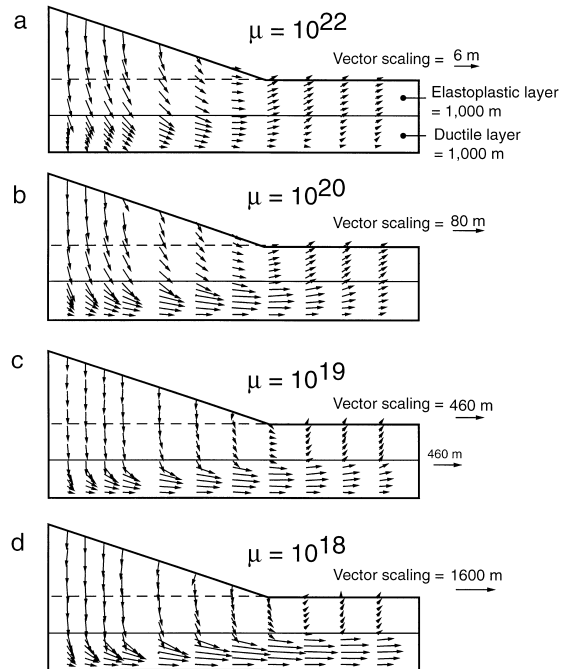
Fig. 4. The effect of changing viscosity in the ductile layer. Displacement vectors for models run with variable viscosity (μ) in the ductile layer. Initial load step, where base of model is prestressed with gravity, is subtracted out leaving only elastic deformation caused by cone load and the time-dependent viscous deformation effects. Scale arrow indicates displacement magnitudes for each run and each run shows displacements over 2 million years. In each experiment the layer is 1000 m thick. (a) $\mu = 10^{22}$ Pa·s; (b) $\mu = 10^{20}$ Pa·s; (c) $\mu = 10^{19}$ Pa·s; (d) $\mu = 10^{18}$ Pa·s.

Table 3

Physical parameters used in the modelling experiments and those parameters estimated for the volcanoes plotted in Fig. 9. D-layer is the thickness of the ductile layer. H is the cone height. EP-layer is the thickness of the elastoplastic layer (in this column volc/number indicates that the elastoplastic layer is thin or non existent). C_v the cohesion of the elastoplastic layer and volcano. Viscosity is the viscosity of the ductile layer. Time is the time taken for the deformation to occur from the initiation of loading

Parameter, symbol and units									Note or reference
radius R $(\times 10^3 \text{m})$	height H $(\times 10^3 \text{m})$	D-layer T $(\times 10^3 \text{m})$	EP-layer D $(\times 10^3 \text{m})$	cohesion C_v	viscosity μ	time t	Πa R/T	Πb $\mu / C_v \cdot D \cdot t$	
Model									
4a	6	2	1	1	9×10^6	10^{22}	2×10^6	6	5.9×10^0	experiment on effect of changing viscosity (Fig. 4a)
4b	6	2	1	1	9×10^6	10^{20}	2×10^6	6	5.9×10^{-2}	experiment on effect of changing viscosity (Fig. 4b)
4c	6	2	1	1	9×10^6	10^{19}	2×10^6	6	5.9×10^{-3}	experiment on effect of changing viscosity (Fig. 4c)
4d	6	2	1	1	9×10^6	10^{18}	2×10^6	6	5.9×10^{-4}	experiment on effect of changing viscosity (Fig. 4d)
5a	6	2	1	1	9×10^6	10^{22}	2×10^6	6	5.9×10^0	experiment on changing ductile layer thickness (Fig. 7a)
5b	6	2	5	1	9×10^6	10^{22}	2×10^6	1.2	5.9×10^0	experiment on changing ductile layer thickness (Fig. 7b)
5c	6	2	10	1	9×10^6	10^{22}	2×10^6	0.6	5.9×10^0	experiment on changing ductile layer thickness (Fig. 7c)
5d	6	2	20	1	9×10^6	10^{22}	2×10^6	0.3	5.9×10^0	experiment on changing ductile layer thickness (Fig. 7d)
6a	6	2	1	2	9×10^6	10^{22}	2×10^6	6	4.4×10^0	2 km thick elastoplastic layer/changing $T = 1000$ m
6b	6	2	5	2	9×10^6	10^{22}	2×10^6	1.2	4.4×10^0	2 km thick elastoplastic layer/changing $T = 5000$ m
6c	6	2	10	2	9×10^6	10^{22}	2×10^6	0.6	4.4×10^0	2 km thick elastoplastic layer/changing $T = 10,000$ m
6d	6	2	20	2	9×10^6	10^{22}	2×10^6	0.3	4.4×10^0	2 km thick elastoplastic layer/changing $T = 20,000$ m
7	3	1	1	1	9×10^6	10^{22}	2×10^6	3	5.9×10^0	small cone 3000 m radius

Volcano										
Concepción	5	1.7	0.5	volc/0.1	10^5	10^{18}	2600	10	7.2×10^0	van Wyk de Vries and Borgia, 1996
Iwaki	5	1.5	4	volc/0.1	10^5	10^{19}	5000	1.25	3.9×10^2	Suzuki, 1968
Fieale	4	0.6	< 4	2	10^6	10^{20}	10,000	> 1	3.9×10^1	μ = our ductile crust estimate
Fantale	5	1	> 5	2	10^6	10^{20}	10,000	< 1	1.1×10^2	μ = our ductile crust estimate
Hawaii 1	600	12	60	40	10^6	10^{20}	4×10^6	0.15	1.5×10^{-2}	Borgia, 1994 (ignoring basal clay layer = flexure due to mantle)
Hawaii 2	100	12	0.5	volc/0	10^6	10^{18}	4×10^6	50	6.6×10^{-4}	Borgia, 1994 (considering only clay layer = ignoring mantle)
Kilimanjaro	30	5	100	volc/1	10^6	10^{22}	1×10^6	0.3	6.3×10^4	volcano on Pan-African crust
Galapagos	50	5	60	10	10^6	10^{20}	1×10^6	0.9	2.1×10^{-1}	1–3 Ma oceanic crust on hotspot mantle
Tjareme	8	2	1	volc/0.5	10^5	10^{18}	1×10^4	8	1.6×10^{-1}	tephra/lava cone on plastic marls (van Bemmelen, 1970)
Urungang	10	2.2	2.5	volc/0.5	10^5	10^{19}	1×10^4	4	1.4×10^2	tephra/lava cone on marine sediments (van Bemmelen, 1970)
Merapi	8	2.1	2	volc/0.5	10^5	10^{18}	5000	4	2.4×10^1	tephra/lava cone on marine sediments (van Bemmelen, 1970)
Socompa	10	3.5	0.5	volc/0	10^7	10^{19}	2×10^5	20	4.5×10^{-2}	thick stubby lava dominated cone (van Wyk de Vries et al., 1997)
Pajonales	15	3.5	0.5	volc/0	10^7	10^{19}	5×10^5	30	4.5×10^{-2}	thick stubby lava dominated cone(van Wyk de Vries et al., 1997)
Etna	20	3	2	volc/0.1	10^6	10^{19}	1×10^6	10	1.1×10^{-1}	estimates derived from Merle and Borgia, 1996
Poas	15	2	0.5	0.2	10^5	10^{19}	5×10^5	30	2.9×10^{-1}	modified estimates from Borgia et al., 1990
Mombacho	6	1.4	0.5	volc/0	10^6	10^{18}	30	12	7.5×10^{-1}	estimates derived from van Wyk de Vries and Francis, 1997
Momotombo	4	1.2	0.5	volc/0	10^5	10^{18}	2	8	1.3×10^2	similar geology to Mombacho, but younger volcano

4. Results

4.1. The influence of varying viscosity

We first consider the effect of changing the viscosity of a ductile layer. We ran four models with a 1000 m thick ductile layer with viscosities of 10^{18}, 10^{19}, 10^{20}, 10^{22} Pa $\cdot$ s. (Fig. 4, Table 3). The plate was 1000 m thick (Table 1).

4.1.1. Displacement

The results show that the magnitude of displacement increases with decreasing viscosity. Thus at 10^{22} Pa $\cdot$ s there is a maximum of 6.4 m movement
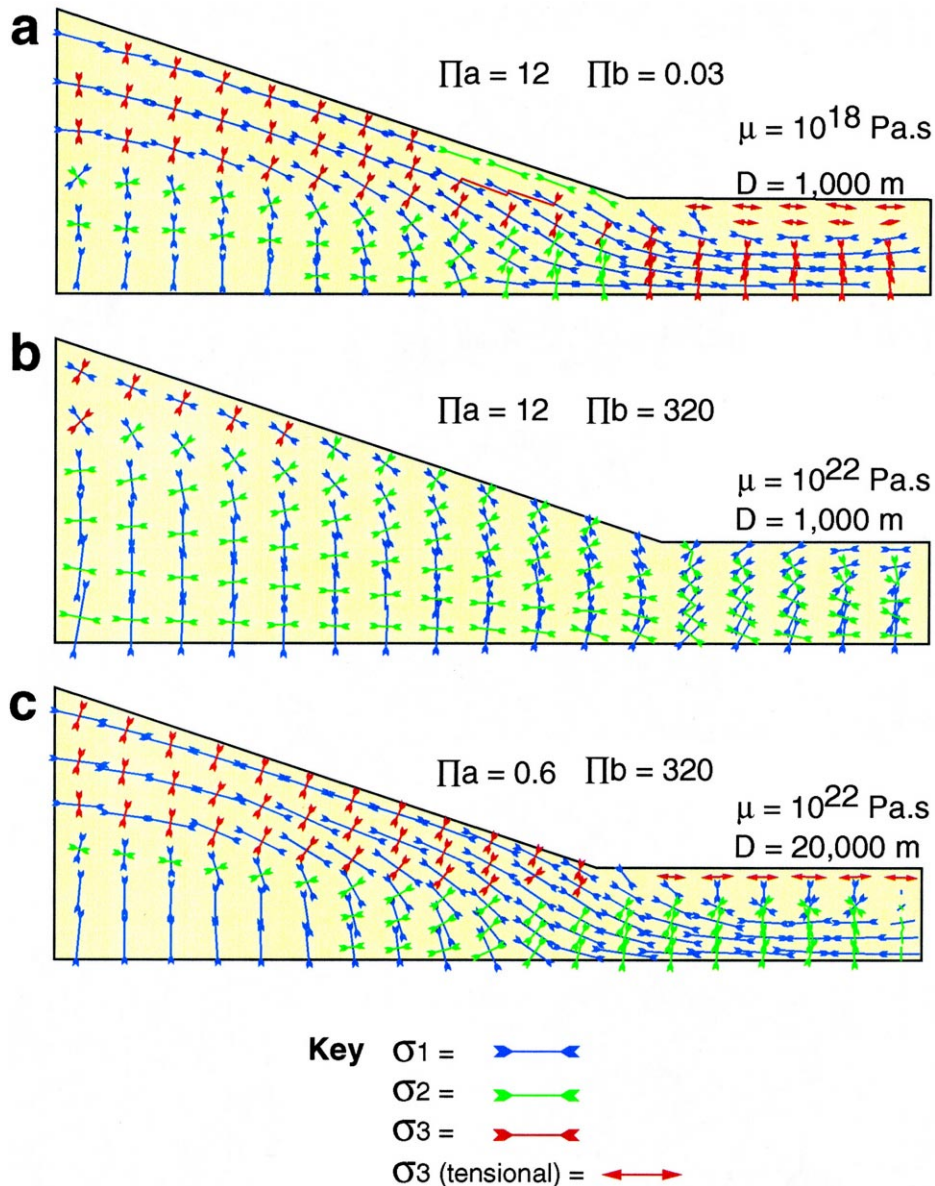
Fig. 5. Principle stress axes in the elastoplastic plate and cone. (a and b) Comparison of 1000 m layer with variable viscosity ($a = 10^{18}$ Pa $\cdot$ s., $b = 10^{22}$ Pa $\cdot$ s.). (b and c) Comparison between 1000 m and 20,000 m thick ductile layer ($b = 1000$ m and $c = 20,000$ m).

(Fig. 4a), while at 10^{18} Pa · s there is 1661 m (Fig. 4d). In addition, the distribution of displacement changes: at high viscosity the greatest movement is in the cone, directed downwards, (Fig. 4a) while at lower viscosities it is concentrated in the viscous layer below the foot of the cone (Fig. 4b). The pattern of flow in the ductile layer also alters with viscosity: at 10^{22} Pa · s, displacement increases upwards from the model base to the elastoplastic plate. In contrast, at lower viscosities there is a parabolic distribution with maximum displacement in the centre of the viscous layer. Lastly, in the cone the horizontal component of movement is outward (positive) at high viscosity (10^{22}–10^{20} Pa · s), but is directed inwards at lower viscosity (10^{19} and 10^{18} Pa · s). At high viscosity therefore, the cone spreads, while at low viscosities it sinks and is compressed, even though the viscous layer is moving outwards by large amounts. At low viscosities the ductile layer is extruded from beneath the cone.

4.1.2. Stresses

Principal stresses within the upper plate and cone are shown in Fig. 5a. Over the whole range of viscosity the stress axes in the cone have similar orientations: σ_1 is slope parallel near the surface, changing to vertical at depth. In the plate σ_1 is mostly vertical at high viscosity, except near the surface, where it tends to become parallel to the surface (Fig. 5b). At lower viscosity, however, a broad region of horizontal σ_1 and vertical σ_3 develops, and near the surface the σ_3 is tensional (Fig. 5a). The intensity of σ_1 increases in the upper cone with decreasing viscosity (compare Fig. 5a and b). In addition, maximum shear stresses increase from 2.7 $\times 10^6$ to 1.9×10^7 Pa (see Fig. 6a and b). The slope parallel compression is a well known feature of volcanic cones involved in flexure (Borgia, 1994).

4.2. The influence of viscous layer thickness

We investigated the effect of changing the thickness of the viscous layer on models with a high viscosity (10^{22} Pa · s). We were unable to run lower viscosity value due to the numerical instabilities of the model. The elastoplastic plate below the volcano cone was kept at 1000 m, while the ductile base thickness (T) was modelled at 1000, 5000, 10,000
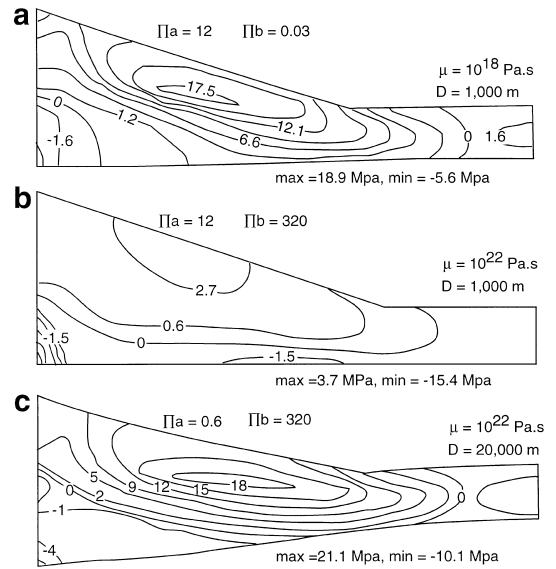
Fig. 6. Shear stresses in the xy plane of elastoplastic plate and cone. (a and b) Comparison of 1000 m layer with variable viscosity ($a = 10^{18}$ Pa·s., $b = 10^{22}$ Pa·s.). (b and c): Comparison between 1000 m and 20,000 m thick ductile layer ($b = 1000$ m and $c = 20,000$ m).

and 20,000 m thickness (Fig. 7, Table 3). With such a high viscosity, our ductile material is analogous to stiff sedimentary rock, volcanic rocks such as lavas and metamorphic rocks. As such, therefore, our models represent the highest viscosity end-member of the possible substrata. The 1000 to 10,000 m runs model the range of possible sedimentary and volcanic substrata thicknesses, while the 5000 to 20,000 km runs model possible involvement of upper to lower crustal rocks in oceanic and continental environments. Greater depths of models where not considered necessary, as the deformation field caused by the volcano became very small at 20,000 m.

4.2.1. Displacement

4.2.1.1. T = 1000 m (Fig. 7a). The 1000-m-thick run is identical to that described in Fig. 4a. The greatest horizontal movement is in the base of the elastoplastic plate and the upper part of the viscous base.

4.2.1.2. T = 5000 m (Fig. 7b). With a ductile layer of 5000 m the flow is still predominantly horizontal and there is more outward spreading movement in
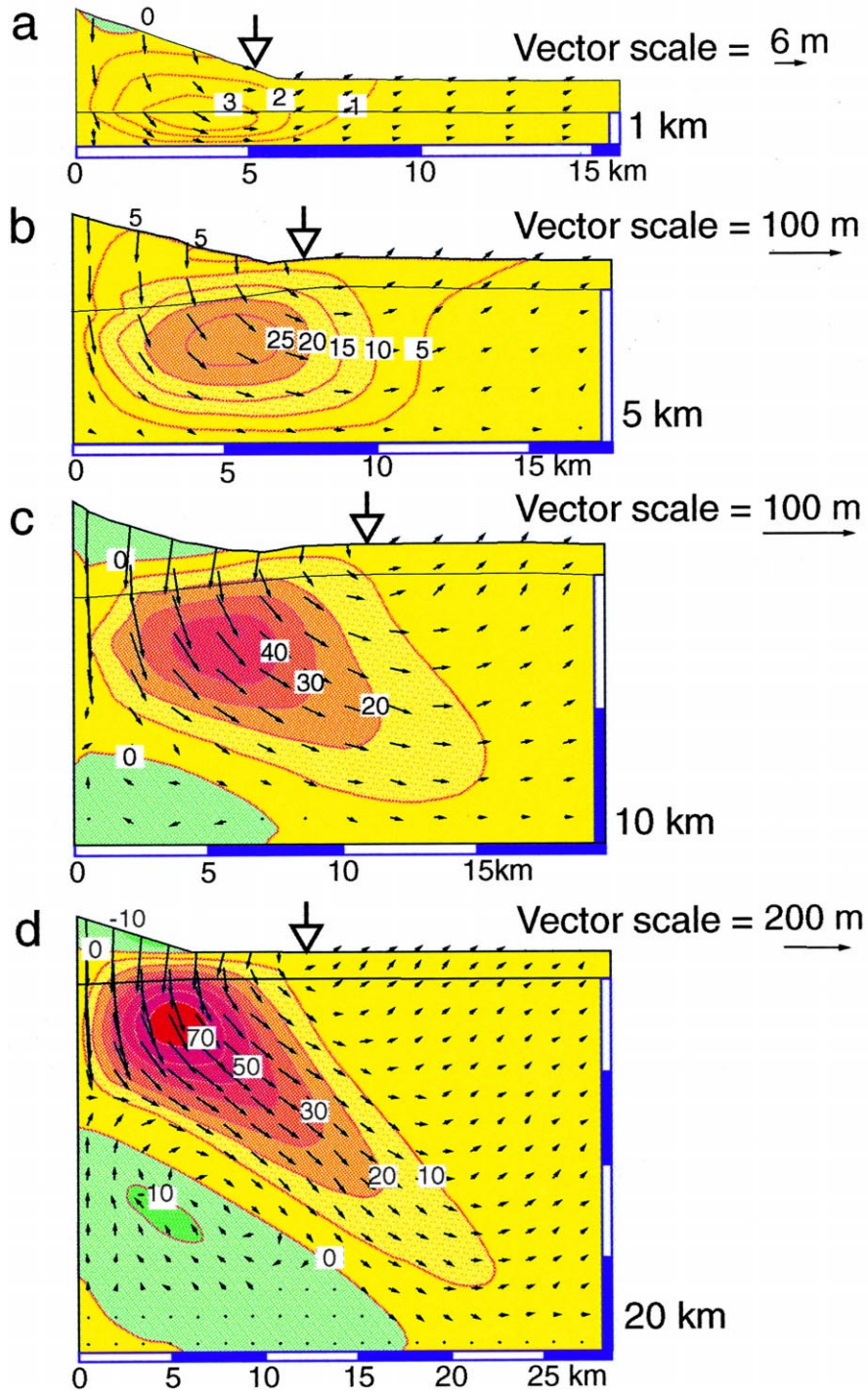
Fig. 7. The effect of changing thickness of the ductile layer. Displacement vectors shown as arrows, with scale bar indicating dimensions. Horizontal displacement values are shown as contours. In each experiment viscosity is held at 10^{22} Pa · s, and all other physical parameters as in Table 1. Note that the deformed shape is included in these diagrams and that the axis of flexure is indicated by an open arrow.

the cone than at 1000 m. The displacement vectors in the fluid form the classic parabolic fluid flow distribution found at low viscosity in the previous experiments.

4.2.1.3. T = 10,000 m (Fig. 7c). At this thickness horizontal vectors of movement are only found near the base of the viscous layer, in the lower 3000 m, while above this the material moves outwards and downwards at about 45° from the base of the elastoplastic layer in a restricted band about 5000 m wide. Above this the amount of displacement is small and changes direction to outward and upward to produce a flexural bulge in the elastoplastic plate. A type of 'recirculation' pattern appears below the main movement band with small inward and upward displacements. We believe this phenomena to be a boundary effect, either caused by the fixed node at the bottom axis of the model, or due to the elastoplastic plate-viscous layer interface. It may be are real effect that occurs in natural systems. There is a very small area of inward movement at the top of the cone.

4.2.1.4. T = 20,000 m (Fig. 7d). A model with a 20,000 m viscous base produces a well developed 45° zone of outward and downward movement, and the 'recirculation' pattern. The amount of displacement in the 45° zone decreases with depth, until at 18,000 m depth it is negligible, indicating that the base no longer has any significant control on the deformation. The whole cone has moved inwards, flexural compression has replaced the spreading seen in the cone on a 1000 m ductile layer.

There is a flexural axis in each model, where the downwards motion of the cone changes to upwards motion of the flexural bulge. The displacement vectors describe a rotational pattern around this axis. With increased thickness of the ductile layer the axis moves outwards from within the cone at 1000 to 5000 m from the cone at 20,000 m (Fig. 7).

4.2.2. Stresses

Principal stresses within the volcano and plate increase in intensity as T increases. At $T = 1000$ m the upper part of the cone has a weak, slope parallel σ_1 of about 3.7×10^6 Pa (Fig. 5b) which increases to 1.8×10^7 Pa at $T = 20,000$ m (Fig. 5c). In addi-

tion, at $T = 20$ km, the slope parallel area of σ_1 extends over the whole cone (Fig. 5c).

On the flexural bulge at the foot of the cone σ_3 is tensional and radial near the surface, similar to the small T, low viscosity run (Fig. 5a). However, lower down σ_3 becomes tangential, and σ_1 is radial: this is the compressed part of the bulge (Fig. 5c). This differs from the thin layer/low viscosity experiments, where σ_1 was vertical and σ_3 horizontal (Fig. 5a). Shear stress in the xy plane is greatest at the surface at low T (Fig. 6b), but it becomes concentrated near the base of the cone about 4 km from the summit in thick T runs (Fig. 6c). It increases in intensity by about one order of magnitude from 2.7×10^6 to 1.75×10^7.

4.3. Additional experiments

The runs above were repeated with an elastoplastic plate of 2000 m. In these runs displacements were smaller, but the deformation pattern was broadly similar, except that the zone of 45° movement was wider and the flexural axis correspondingly further from the base of the cone due to the a larger flexural wavelength.

We also ran an experiment with a cone half the size of that used in the main experiments, i.e. 1000 m high and 3000 m radius. This experiment used a 1000 m plate and a 10,000 m ductile base. The resulting deformation was similar to a 2000 m volcano on a 20,000 m base, indicating that the style of deformation in the ductile layer varies in proportion to the size of the cone.

5. Discussion: the parameters affecting styles of deformation

The models presented here show that changes in the thickness and viscosity of a ductile region below a volcano can result in different deformation states. We use two dimentionless Π-numbers to describe the nature of these effects. One number, Π_a, has already been introduced when discussing the simple analogue model. It is the ratio of the volcano radius to ductile substratum thickness. The second number Π_b, is the ratio of the viscosity of the ductile layer

(μ) to an approximation to the cohesive strength of the cone and plate:

$$\Pi b = \mu/c_v \cdot (D + H) \cdot t,$$

where is c_v is the cohesion of the cone, D the thickness of the elastoplastic layer, H the height of the cone and t, the time after volcano emplacement.

This number has similarities to the Π_6 used in the analysis of the analogue experiments of Merle and Borgia (1996), although they considered a cohesionless, Coulomb–Navier failure criterion, and used the failure resistance force, where we use the cohesion. We consider that between different volcanoes and substrata the angle of friction is likely to vary little ($\sim 30°$), but that the cohesion is likely to vary over several orders of magnitude. For example, a volcano may sit on cohesionless sands or strongly cohesive crystalline rocks. In addition (as is discussed below), the cohesion of the volcano can vary widely depending on the material out of which it is constructed, and if it is faulted or not. As the cohesion is therefore the controlling factor in the failure strength of the volcano and elastoplastic plate, for this simple analysis we use it alone, and ignore other constant parameters. We only vary the cohesion and D and H in the analysis here.

5.1. Variable Π_b: changing the ductile layer viscosity

When considering a thin ductile layer (e.g. the experiments shown in Fig. 4), there are two modes of deformation: volcano and substratum spreading and basement extrusion. In our experiments their occurrence depends on the viscosity of the ductile substratum, which affects the amount of coupling between the ductile layer and the overlying elastoplastic plate/volcano. This relationship is depicted using Π_b, where the numerator (μ) is the only variable in the experiments.

5.1.1. Volcano and substratum spreading

This occurs where the basal ductile layer is well coupled with the volcano/plate, i.e. when viscous forces are large compared with the failure strength of the volcano/plate (Fig. 8a): if the Π_b is high. In this case the ductile material will drag the volcano and plate outwards as seen in Fig. 4a. The volcano
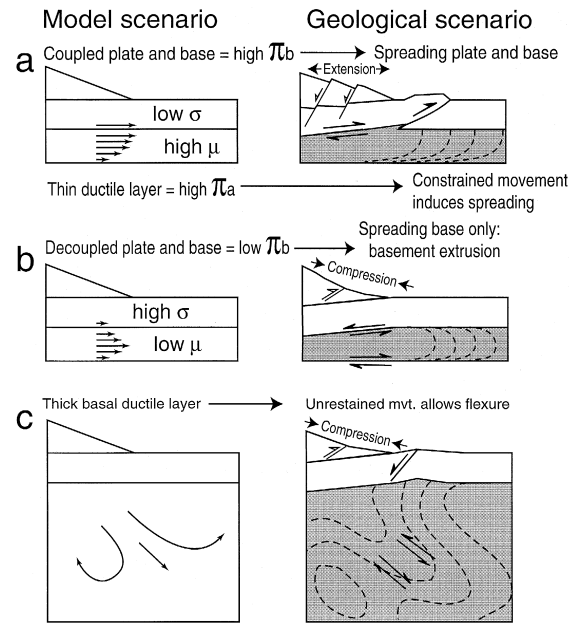
Fig. 8. Schematic diagram explaining the effect of different amounts of coupling between volcano and substratum and effect of changing ductile layer thickness. (a) A system with a thin ductile layer: a high Π_a. In this case the thin ductile layer and a high Π_b results in a spreading volcano. The cone is extended creating normal faults which inhibit sector collapse formation. The ductile layer may be sedimentary rocks, pyroclastics, or oceanic crust containing hydrothermal activity/partial melt. (b) A similar system to (a), but with a low Π_b, which results in substratum extrusion and a compressed volcano. The compression results in high slope-parallel stresses, thrust formation and high collapse potential. For such a scenario, soft sediments are the most likely substrata (low μ), and/or there may be a strong volcano. (c) A similar situation as in (a), but with a thick ductile layer, (low Π_a), which results in flexure. Such a thick substratum could either be thick sedimentary sequences (as at Iwaki), oceanic mantle, ductile lower crust. this situation could also be produced on stiffer crust over long time periods.

and plate below it are stretched horizontally and extended, while the plate at the edge of the volcano will be compressed. If both can fail by faulting, the volcano will display normal faults and the plate will develop thrust faults.

5.1.2. substratum extrusion

This occurs where the viscosity of the ductile base is low compared with the volcano/plate resistance (Fig. 8b). The Π_b is low. In this case there is less coupling of the two layers and ductile basement is

extruded outwards. It still causes drag on the plate, pulling the lower part outwards, but as material is removed from under the volcano, the cone sags downwards and is put into compression.

5.2. Volcano cohesion and ductile layer coupling (Π_b)

In our experiments we varied the viscosity of the basal layer, altering Π_b and the degree that the base was coupled to the volcano. The coupling ability of the system also depends on the strength of the plate. The lower the cohesion, the more coupling is possible. In addition, a thicker plate will couple less, as increased thickness makes it stiffer.

At the relatively low viscosities of clayey sediments, 10^{17}–10^{18} Pa $\cdot$ s, (van Wyk de Vries and Borgia, 1996) the cohesion of the volcano is likely to be an important factor in determining which type of deformation occurs. The variation in cohesive strength of volcanoes has not been studied in any depth. However, we suggest that strength may vary by large amounts with the ratio of lava to tephra in the edifice. A lava dome will have a high cohesion, whereas a tephra cone may be nearly cohesionless. Stratovolcanoes can be tephra dominated, such as Concepción (van Wyk de Vries and Borgia, 1996), or they may be lava dominated, such as the steep andesitic–dacitic cones in the Andes (Francis and Wells, 1988). On a similar substratum the tephra-dominated cones are more likely to couple and spread than stronger lava-dominated cones.

In the Andes, there is copious evidence of spreading below Pajonales and Socompa volcanoes, but no clear evidence of spreading in the cone (van Wyk de Vries et al., 1997). These may therefore be natural cases of basement extrusion. In contrast, at Concepción and Maderas in Nicaragua, even though the substratum is of very low viscosity ($\mu = 10^{15\text{-}18}$ Pa $\cdot$ s) the tephra-dominated cones spread (van Wyk de Vries and Borgia, 1996).

Our models are simplified compared with actual geological situations. In particular while we consider a single plate and ductile layer system, most volcanoes stand on layered sequences of rock which may contain many potential ductile layers and decollements. The presence of decollements may decrease the apparent viscosity of the basement in a horizontal plane, promoting spreading. It is possible with our modelling to decide from field data whether a basement behaves as one ductile entity throughout (flexure) or as a layered one (spreading).

5.3. Variable Π_a: changing the ductile layer thickness

A comparable range of displacements and stress fields are produced by changing the thickness of the ductile layer (T) (Fig. 8c). As in the analogue experiment, changing T alters the Π_a of the system. At low values of T, displacement in the viscous layer is predominantly horizontal, as it is confined between narrow boundaries. Spreading or basement extrusion are the dominant deformation styles. At low Π_a, the fluid layer is not constrained by its boundaries and there is a significant component of vertical displacement. This leads to formation of a flexural bulge, and very strong compressive stresses in the volcano.

In the experiments described in Fig. 7, the outward spreading of volcano and plate changes to inwards flexure between the 5000 and 10,000 m runs. This equates to a Π_a of between 1.2 and 0.6, a value encompassing that of the analogue experiment.

5.3.1. Volcano size

The single experiment with a cone 1000 m in height and 3000 m in radius illustrates that the size of the volcano plays a role in the style of deformation (Fig. 8d). With a smaller volcano, the thickness of ductile layer required to accommodate vertical deformation is less. This relationship can be again expressed as the dimensionless number Πa.

If a substratum of a certain thickness is considered, then small volcanoes may not produce enough load to cause significant deformation. However if they do, they will tend to undergo flexure due to their low Π_a. In contrast larger cones with high Π_a may spread. This means that as a volcano grows it may cause different styles of deformation. It will first tend to cause flexural deformation since Π_a is small, but as it grows Π_a will increase, the base of the ductile layer will begin to interfere with the deformation, and horizontal flow will predominate.

Interestingly, as a volcano spreads its Π_a will increase, and the system will become geometrically more 'spreadable'. However, this effect is opposed

by the decrease in available gravitational potential as the volcano height is reduced (reducing the Π_1 of Merle and Borgia, 1996). An implication of this interpretation of the role of Π_a is that for edifices of the same volume, shields are more likely to spread, while steep cones will be more prone to flexure.

5.4. Spreading, extruding and flexing volcanic fields

The two parameters Π_a and Π_b can be plotted against each other to produce a diagram illustrating the possible fields of deformation for volcanoes of different sizes on different basements (Fig. 9). Three fields of flexural deformation, spreading and extrusion have been delimited on the diagram. When the Π_a ratio is small, flexural deformation operates while at higher Π_a ratios, spreading or extrusion occur. At low Π_b, basement extrusion is dominant and at higher Π_b ratios, cones spread with the basement.

We plot our volcano examples from Fig. 1 onto Fig. 9. The structure of Concepción indicates that it lies within the spreading or extrusion fields. The extrusion of basement at Concepción is a conspicuous process, but spreading structures are also found on the cone. At Concepción, about 500 m of plastic Quaternary lake clays lie on Tertiary marine flysh
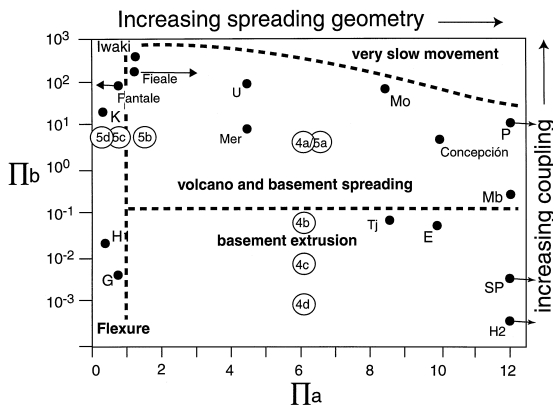
Fig. 9. Plot of Π_a against Π_b illustrating the approximate fields occupied by flexure, spreading and extrusion dominated systems. Model runs from this paper plotted on this diagram, as well as the runs of Merle and Borgia (1996). Natural examples mentioned in the text are also plotted. These include Kilimanjaro (K); Hawai'i (H1 = with mantle; H2 = only considering basal sediment layer); Galapagos (G); Etna (E); Javan volcanoes Tjereme (Tj), Merapi (Mer) and Urungang (U); Poas (P); Socompa/Pajonales (SP); Mombacho (Mb) and Momotombo (Mo).

(Table 3), with the clays acting as a low viscosity ductile layer (van Wyk de Vries and Borgia, 1996). Thus Concepción probably lies on the border between volcano and basement extrusion and coupled spreading.

The structure of Iwaki indicates that the volcano lies within the flexure field. Suzuki (1968) indicates that the basement at Iwaki consists of 4000 m Pliocene and Miocene marine sediments, which may provide the thick viscous layer. As the radius of the cone is about 5 km, Π_a is about 1.25, just outside the flexure field of Fig. 9.

The structure of Fieale is indicative of a spreading or extruding basement. At the volcano, the top few km of the crust are composed of basaltic lava (De Chabalier, 1993), which probably behaves as the elastoplastic plate (Table 3). In order to produce the observed deformation there must be a ductile layer below this of less than 5000 m thickness. This is probably composed of rock at elevated temperatures, possibly containing magma and active hydrothermal systems, both of which will tend to reduce the effective viscosity of the rocks.

At Fantale the fault pattern indicates a flexure-dominated system. We know little about the basement at Fantale but can predict that the ductile layer must be very thick compared with the volcano: a Π_a of more than 1, equivalent to a ductile layer thickness of at least 10,000 m (Table 3). This indicates that in contrast to Fieale, there must be some thick layer that can deform viscously. Such a thick layer is unlikely to be sedimentary, but may be ductile mid to lower crust. We plot the possible range of values for these two volcanoes on Fig. 9.

In addition we plot some other volcanoes and volcanic basement types on the diagram in Fig. 9.

5.4.1. Volcanoes in the flexure field: $\Pi a < 1$

At one end of this field are highly coupled systems (high Π_b), such as volcanoes on thick high-viscosity continental metamorphic basement. We pick Kilimanjaro and Mt. Kenya as examples, as they have basal bulges and compressed edifices (van Wyk de Vries and Borgia, 1996). While such crust is not generally considered as a viscous material our experiments indicate that at viscosities as high as 10^{22} Pa·s there can be significant deformation within 2 million years: the lifetime of such large edifices.

At lower Π_b are intraplate seamounts, such as those of the Galapagos and Canary Islands, which are resting on oceanic crust (elastoplastic plate) and mantle (ductile layer). The Hawaiian chain would also be in this field but for the thin clay layer below them which gives a high Π_a (Nakamura, 1980).

5.4.2. Extrusion field: low Π_b and high Π_a

Volcanoes standing on sedimentary or pyroclastic sequences may plot in this field, especially the stronger lava dominated cones. Examples for this field are Socompa and Pajonales, Chile (van Wyk de Vries et al., 1997) and Tjareme, Java (van Bemmelen, 1970), Mt. Etna (Borgia et al., 1992) and possibly Mombacho, Nicaragua (van Wyk de Vries and Francis, 1997).

5.4.3. Spreading field: high Π_b and high Π_a

This contains volcanoes on sedimentary sequences, especially those in basins, erupted onto recent sediments, or recently uplifted marine sequences. Tephra-dominated cones with low cohesion also fall into this category (where Π_b is high). Examples are Merapi and Urungang volcanoes, Java (van Bemmelen, 1970) and Poas, Costa Rica (Borgia et al., 1990). In this area too, we plot volcanoes on young oceanic crust, i.e. near ridges. In such locations there may be a thin low viscosity layer in the mantle or crust, caused by hydrothermal activity or partial melt. Examples of these are Axial volcano and Fieale (van Wyk de Vries and Merle, 1996a).

5.5. Implications of extrusion tectonics to volcano collapse

The amount of coupling of base and volcano/plate (Π_b) has important implications for the stability of spreading volcanoes. Well coupled volcanoes will be pulled apart to form distinctive leaf graben type normal faults (Merle and Borgia, 1996), while poorly coupled volcanoes will be placed under compression as they sink and bend (Fig. 9). van Wyk de Vries and Borgia (1996) showed that at radially spreading volcanoes, such as Concepción, spreading would result in a reduced likelihood of sector collapse by relaxing stresses in the cone, reducing slope angles and producing inward dipping fault planes. In other situations, where coupling is low and extrusion is occurring, compressive stresses will be high in the cone, stress trajectories favour outward dipping faults and slope angles do not decrease. Thus, with increasing decoupling there may be an increasing risk of flank failure, especially if one sector of the volcano is preferentially spreading (van Wyk de Vries and Francis, 1997). The volcano collapse at Socompa involved spreading basement (van Wyk de Vries et al., 1997) but the volcano lacks extensional structures in the cone, raising the possibility that the system was extruding basement before collapse occurred.

6. Conclusions

We have described natural examples of two styles of volcano gravitational deformation: volcano flexure and volcano spreading. Our modelling indicates that these are a product of deformation of a ductile basement layers with different thickness and viscosity. If the ductile layer is very thin compared with the volcano ($\Pi_a > 1$) then spreading occurs, while if the layer is thick, flexure occurs ($\Pi_a < 1$). By changing the viscosity of the basal ductile layer we show that the spreading type of deformation can be subdivided into spreading and extruding systems, characterised by the ratio of viscosity to failure strength (Π_a). In volcano spreading systems, the volcano is effectively coupled to the basal layer (high Π_b) and is dragged outwards with it. In extruding systems (low Π_b), the basal layer is less coupled to the cone, and the base flows outwards while the volcano sinks downwards.

By plotting the coefficient of spreading potential (Π_a), against coupling (Π_b) we produce a graph illustrating the structural styles of possible combinations of volcano size, ductile layer thickness and viscosity. Knowledge of basement geology allows the deformation style at a volcano to be predicted. Such predictions may be used in assessing the collapse potential of a volcano, and in assessing activity state. Conversely, if the deformation style at a volcano is known then predictions can be made about the type of basement below it. This is especially useful for planetary geology, and where field observations are not possible.

We have used the method to predict the presence of a thin (< 5000 m) ductile layer below Fieale volcano, and a thick (+ 10,000 m) one below Fantale. We propose a thin, low viscosity layer below Iceland to account for spreading features there. We also suggest that the Venusian arachnid structures may indicate the presence of thin ductile layers in the crust of that planet.

Acknowledgements

References

ANSYS, 1996. Users reference manual 5.3, Houston, PA.

Baguley, D., Hose, D.R., 1994. How to Chose a Finite Element Pre and Post Processing. NAFEMS, Glasgow.

Borgia, A., 1994. The dynamic basis of volcanic spreading. J. Geophys. Res. 99, 17791–17804.

Borgia, A., Burr, J., Montero, L.D., Morales, W., Alvarado, G.E., 1990. Fault propagation folds induced by gravitational failure and slumping of the Central Costa Rica Volcanic Range: Implications for large terrestrial and Martian volcanic edifices. J. Geophys. Res. 95, 14357–14382.

Borgia, A., Ferrari, L., Pasquare, G., 1992. Importance of gravitational spreading in the tectonic and volcanic evolution of Mount Etna. Nature 357, 231–235.

Borgia, A., van Wyk de Vries, B., Mbasha, M., 1994. A structural study of Kilimanjaro. Magmatic Processes 1995: Do The Answers Lie in the Rocks? Volcanic Studies Group meeting, Sheffield, 4–6 January, 1995. Geological Society London, 15 pp.

Cyr, K.E., Melosh, H.J., 1993. Tectonic patterns and regional stresses near Venusian Coronae. Icarus 102, 175–184.

De Borst, R., 1982. Calculation of collapse loads using higher order elements. In: Wermeer, P.A., Luger, H.J. (Eds.), Deformation and Failure of Granular Materials. A.A. Balkema. Rotterdam, pp. 503–513.

De Chabalier, J.-D., 1993. Topographie et déformation tridimensionnelle du rift d'Assal (Djibouti): De la disparition d'un volcan á la naissance d'un océan. Ph.D. thesis, Paris 7.

De Chabalier, J.-D., Avouac, J.-P., 1994. Kinematics of the Asal Rift (Djibouti) determined from the deformation of Fieale volcano. Science 265, 1677–1681.

Francis, P.W., Wells, G.L., 1988. Landsat thematic mapper observations of debris avalanche deposits in the Central Andes. Bull. Volcanol. 50, 258–278.

Merle, O., Borgia, A., 1996. Scaled experiments of volcanic spreading. J. Geophys. Res. 101, 13805–13817.

Middleton, G.V., Wilcock, P.R., 1994. Mechanics in the Earth and Environmental Sciences. Cambridge University Press, Cambridge, 267 pp.

Nakamura, K., 1980. Why do long rift zones develop in Hawaiian volcanoes. A possible role of thick oceanic sediments. Bull. Geol. Soc. Jpn. 25, 255–267.

Suzuki, T., 1968. Settlement of volcanic cones. Bull. Volcanol. Soc. Jpn. 13, 95–108.

van Bemmelen, R.W., 1970. The Geology of Indonesia volume 1A General Geology of Indonesia and Adjacent archipelagoes, 2nd ed. Martinus Nijhoff, The Hague.

van Wyk de Vries, B., Francis, P.W., 1997. Catastrophic collapse at stratovolcanoes induced by slow volcano spreading. Nature 387, 387–390.

van Wyk de Vries, B., Borgia, A., 1996. The role of basement in volcano deformation. In: McGuire, W.J. et al. (Eds.), Volcano Instability on the Earth and other Planets. Geol. Soc. London Spec. Publ. 110, 95–110.

van Wyk de Vries, B., Merle, O., 1995. The effect of volcanic edifices on rifting. IUGG XXI General Assembly, Vol. A. IUGG, Boulder, CO, p. 472.

van Wyk de Vries, B., Merle, O., 1996a. The effect of volcano constructs on rift fault patterns. Geology 24, 643–646.

van Wyk de Vries, B. Merle, O., 1996b. The Iceland Volcano: Analogue Answers. Volcanic Studies Group meeting, Bristol 4–6 January. Geological Society, London, 21 pp.

van Wyk de Vries, B., Self, S., Francis, P.W., 1997. Did Socompa collapse or did it fall?. J. Conf. Abstr. 2 (1), 78.

Zienkiewicz, O.C., 1977. The Finite Element Method. McGraw-Hill, London.